Chinese Chemical Letters 37 (2026) 112890

Contents lists available at ScienceDirect

Chinese Chemical Letters

journal homepage: www.elsevier.com/locate/cclet

Chiroptical properties and supramolecular chirality transfer in a bilayer spironanographene

Zhaoyu Yan, Yuanhao Feng, Zhewen Ma, Wei Zheng*

Interdisciplinary Materials Research Center, School of Materials Science and Engineering, Tongji University, Shanghai 201804, China

ARTICLE INFO

Article history:
Received 6 March 2026
Revised 29 April 2026
Accepted 5 May 2026
Available online 6 May 2026

Keywords:
Bilayer spironanographene
π-Surface recognition
Supramolecular assembly
Circularly polarized luminescence
Supramolecular chirality transfer

ABSTRACT

Bilayer nanographenes represent an emerging class of molecular carbon architectures that provide unique opportunities to explore interlayer electronic communication and chiroptical phenomena in confined π-systems. However, the development of well-defined chiral bilayer nanographenes capable of transferring chirality across extended π-surfaces and supramolecular assemblies remains challenging. Herein, we report the synthesis and structural characterization of a chiral bilayer spironanographene (**spiro-NG**) composed of two nanographene subunits connected through a rigid spirobifluorene core. Single-crystal X-ray diffraction reveals a folded bilayer geometry that enforces significant interlayer π-overlap while simultaneously generating intrinsic molecular chirality. Enantiomeric resolution affords configurationally stable *P*- and *M*-**spiro-NG**, which display pronounced circular dichroism (CD) and circularly polarized luminescence (CPL). Furthermore, the exposed π-surfaces of the bilayer scaffold enable π-surface recognition with coronene, leading to hetero-π stacked co-crystals that highlight the supramolecular adaptability of the nanographene framework. Notably, supramolecular co-assembly of **spiro-NG** with achiral fluorophores enables chirality transfer through Förster resonance energy transfer, resulting in induced CPL emission with tunable wavelengths. These findings establish bilayer spironanographene as a versatile chiral nanographene platform that integrates structural chirality, supramolecular recognition, and chiroptical functionality, offering new opportunities for the development of chiral carbon-based photonic materials.

© 2026 Published by Elsevier B.V. on behalf of Chinese Chemical Society and Institute of Materia Medica, Chinese Academy of Medical Sciences.

Bilayer nanographenes have recently emerged as an important class of molecular carbon architectures for investigating electronic communication in confined π-systems [1]. In contrast to monolayer nanographenes, bilayer structures contain two closely spaced π-surfaces whose relative orientation and separation can be precisely controlled through molecular design [2]. Such structural features enable strong interlayer electronic coupling, which can give rise to unusual optical and electronic properties, including excimer-like emission, charge-transfer interactions, and tunable electronic structures [3–11]. Because of these characteristics, bilayer nanographenes are increasingly regarded as well-defined molecular models for exploring the fundamental physics and chemistry of stacked graphene systems [12,13].

Beyond their electronic properties, bilayer nanographenes also provide unique opportunities for generating molecular chirality in extended π-conjugated systems [14–16]. Chirality can arise when two π-surfaces adopt a nonplanar arrangement that lacks mirror symmetry, leading to distinct enantiomeric structures [17,18]. In recent years, chiral nanographenes have attracted growing attention because they can exhibit strong circular dichroism (CD) and circularly polarized luminescence (CPL), which are highly desirable for applications in chiral optoelectronics, photonic devices, and bioimaging [19–30]. Various structural strategies have been developed to introduce chirality into nanographene frameworks, including helicene-like twisting, nonplanar polycyclic aromatic hydrocarbons, and spiro-connected architectures [31–43]. Among these approaches, spirojunctions offer a particularly attractive strategy for constructing chiral π-systems [44]. The rigid orthogonal connection imposed by the spirocenter can generate stable stereogenic frameworks while maintaining extended conjugation within each aromatic unit [45]. When large polycyclic aromatic hydrocarbons are integrated into such architectures, the resulting systems may enable efficient chirality transfer from the stereogenic core to extended π-surfaces, leading to amplified chiroptical responses [46–48]. Despite these advantages, examples of structurally defined chiral bilayer nanographenes based on spiroarchitectures remain relatively limited.

In addition to their intrinsic chirality, nanographenes possess large exposed aromatic surfaces that can engage in π–π recognition with other aromatic molecules [49]. Such π-surface

* Corresponding author.
E-mail address: zhengwei@tongji.edu.cn (W. Zheng).

https://doi.org/10.1016/j.cclet.2026.112890
1001-8417/© 2026 Published by Elsevier B.V. on behalf of Chinese Chemical Society and Institute of Materia Medica, Chinese Academy of Medical Sciences.

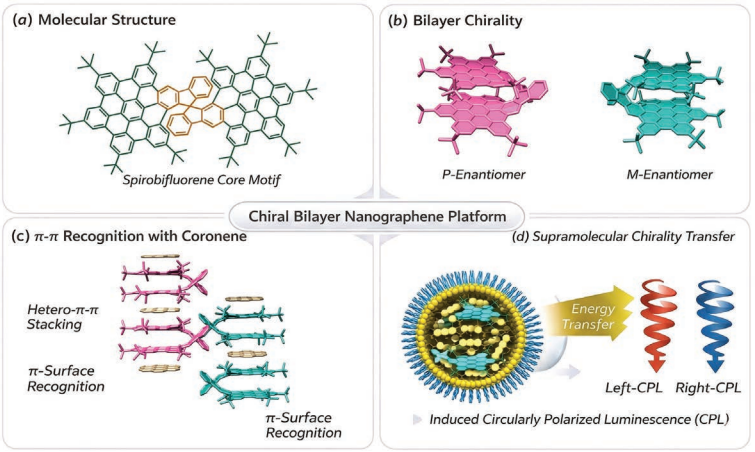


Fig. 1. (a) Molecular structure of the bilayer nanographene featuring a spirobifluorene core motif that enforces a rigid chiral axis. (b) Bilayer chirality of the nanographene scaffold, giving rise to two enantiomeric configurations (*P* and *M*). (c) Supramolecular π–π recognition between the nanographene platform and coronene molecules. Side views illustrate hetero-π–π stacking interactions, while the complementary aromatic surfaces enable effective π-surface recognition. (d) Schematic illustration of supramolecular chirality transfer within vesicular assemblies. Encapsulation of the chiral nanographene platform and guest dyes allows energy transfer processes that induce CPL, generating left- and right-handed CPL signals.

interactions play an important role in supramolecular chemistry, influencing molecular packing, electronic coupling, and photophysical behavior [50–54]. In particular, interactions between different nanographene units can lead to hetero-π stacked architectures, which provide useful platforms for modulating electronic and optical properties [55–58]. However, the ability of bilayer nanographenes to participate in controlled π-recognition with external nanographene guests remains largely unexplored. Another emerging direction in chiral nanographene research involves the supramolecular transfer of chirality [59–62]. In such systems, a chiral chromophore can act as a donor that transfers its chiral information to achiral luminophores through energy-transfer processes [63–66]. This strategy provides a powerful approach for generating induced CPL with tunable emission wavelengths. Nevertheless, molecular systems capable of simultaneously integrating intrinsic chirality, supramolecular recognition, and energy-transfer-mediated chirality transfer remain scarce.

Herein, we report a chiral bilayer spironanographene (**spiro-NG**) that integrates two nanographene subunits through a rigid spirobifluorene core (Fig. 1a). Single-crystal X-ray diffraction reveals a folded bilayer geometry with significant interlayer π-overlap, while the rigid architecture gives rise to intrinsic molecular chirality that can be resolved into enantiopure *P*- and *M*-**spiro-NG** (Fig. 1b). The isolated enantiomers display pronounced circular dichroism and circularly polarized luminescence. Moreover, the exposed π-surfaces enable π-recognition with coronene, leading to hetero-π stacked co-crystals that highlight the supramolecular adaptability of the bilayer scaffold (Fig. 1c). Finally, supramolecular co-assembly with achiral fluorophores enables energy-transfer-mediated chirality transfer, producing tunable CPL emission (Fig. 1d). These results establish bilayer spironanographenes as versatile platforms for constructing chiral nanographene-based supramolecular photonic materials.

The bilayer spironanographene (**spiro-NG**) was synthesized through a modular strategy that integrates a rigid spirobifluorene core with preorganized polyphenylene precursors, followed by a final oxidative cyclodehydrogenation. Although the molecular structure of **spiro-NG** was recently reported by Martín and colleagues in the context of its reduction-induced C–C bond cleavage [67], our group had independently designed and completed the synthesis of this target through the distinct route presented here before their publication. As outlined in Fig. 2a, double Sonogashira coupling of 2,2′-dibromo-9,9′-spirobi[9*H*-fluorene] **1** with 4–*tert*-butylphenylacetylene afforded the corresponding dialkyne intermediate, which subsequently underwent a double Diels–Alder cycloaddition with tetrakis(4–*tert*-butylphenyl)cyclopentadienone. Spontaneous extrusion of carbon monoxide yielded the polyphenylene precursor **4**, which was efficiently planarized under $FeCl_3$-mediated oxidative cyclodehydrogenation to afford **spiro-NG**. The molecular structure of **spiro-NG** was unambiguously confirmed by ^1H (Fig. 2b and Fig. S4 in Supporting information) and ^{13}C NMR spectroscopy (Fig. S5 in Supporting information) as well as high-resolution mass spectrometry (Fig. 2c), indicating the successful formation of the fully fused bilayer framework.

Single-crystal X-ray diffraction analysis unequivocally revealed the bilayer architecture of **spiro-NG**. Suitable single crystals were obtained by slow vapor diffusion of methanol into a dichloromethane solution. As shown in Fig. 3a, **spiro-NG** adopts a rigid spirocyclic framework in which the two fused five-membered rings define a dihedral angle of 76.8°, enforcing a folded bilayer topology. This geometry brings the two hexa–peri-hexabenzocoronene subunits into close proximity, resulting in a partially overlapped arrangement reminiscent of AA-type stacking in bilayer graphene. A top-view projection indicates significant interlayer overlap involving ten conjugated rings, while the mean interlayer distance is 3.5 Å, consistent with values reported for closely coupled bilayer nanographenes (Fig. 3b). The crystal lattice contains a racemic mixture of *P*- and *M*-enantiomers, with homochiral molecules aligning unidirectionally along the *a*-axis (Fig. 3c). Importantly, in the neutral state, extensive intermolecular π–π stacking is effectively suppressed by the peripheral *tert*–butyl substituents, which act as steric spacers and isolate individual bilayer units in the solid state.

To further investigate the accessibility of the π-surfaces of the bilayer nanographene framework, we explored its ability to recognize external aromatic guests through π–π interactions. In particular, coronene, a prototypical planar nanographene with a well-defined hexagonal π-surface, was selected as a model guest molecule due to its complementary size and strong π-stacking propensity. Slow vapor diffusion of methanol into a dichloromethane solution containing **spiro-NG** and coronene afforded high-quality co-crystals suitable for single-crystal X-ray diffraction analysis. Structural analysis revealed the formation of a well-defined **spiro-NG**/coronene co-crystal, demonstrating a clear example of π-surface recognition between two nanographene

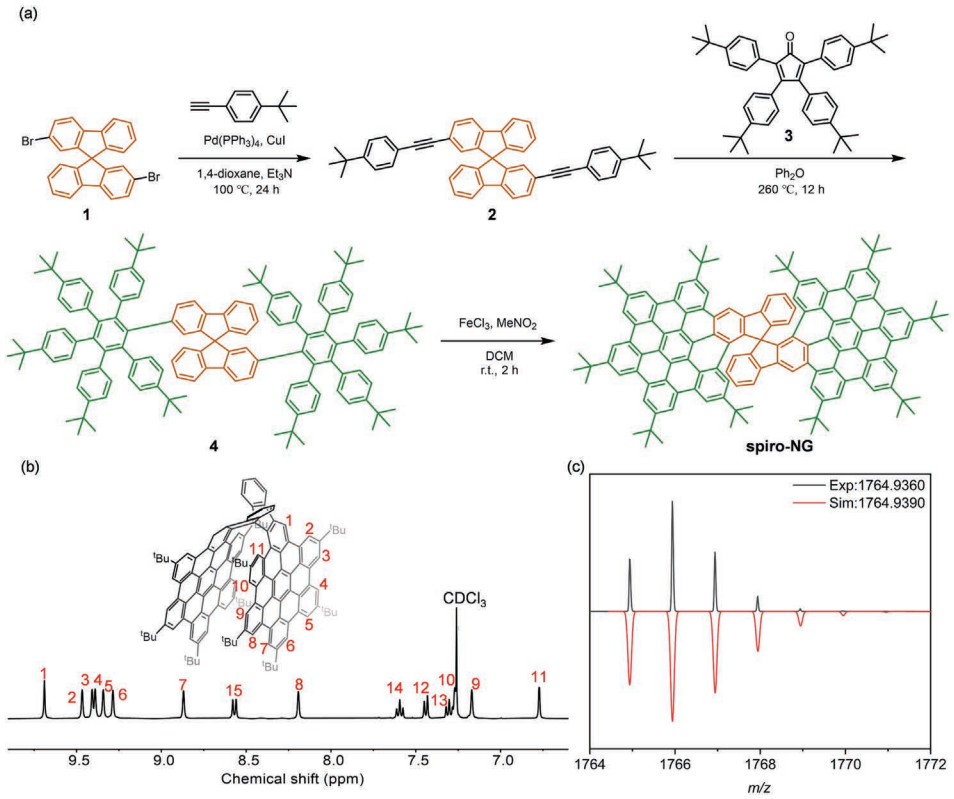


Fig. 2. Synthesis and characterization of **spiro-NG**. (a) Synthetic route to **spiro-NG**. (b) Partial ^{1}H NMR spectrum (400 MHz, $CDCl_3$, 298 K) of **spiro-NG:** The well-resolved aromatic signals and their corresponding assignments (1–15) confirm the highly symmetric structure and successful cyclization of the nanographene subunits. (c) High-resolution MALDI-TOF mass spectrum of **spiro-NG**.

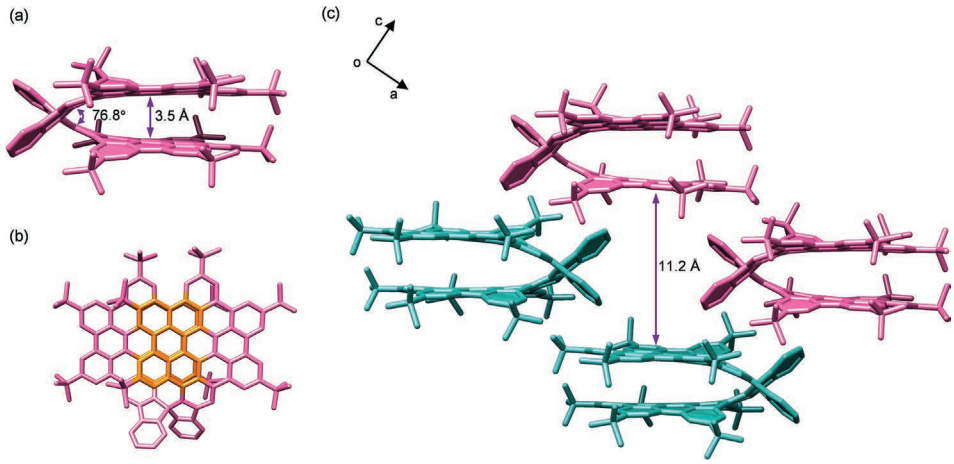


Fig. 3. X-ray crystallographic structure and packing analysis of **spiro-NG**. (a) Side view of the *P*-**spiro-NG** bilayer. (b) Top view highlighting the π-π interaction area: The overlapping region between the two nanographene decks consists of 10 benzene rings (highlighted in orange), providing a substantial platform for electronic communication and structural stability. (c) Perspective view of the crystal lattice showing the 3D arrangement of **spiro-NG** molecules.

systems. In the co-crystalline structure, the bilayer geometry of **spiro-NG** remains largely unchanged, preserving the folded topology imposed by the spirocyclic core. Remarkably, coronene molecules are located in the intermolecular space between neighboring **spiro-NG** units, where they engage in face-to-face π–π interactions with the exposed aromatic regions of the nanographene subunits (Fig. 4a).

The centroid-to-plane distances between coronene and the adjacent nanographene surfaces are approximately 3.4–3.5 Å, which fall within the typical range for π–π stacking interactions in extended polycyclic aromatic hydrocarbons (Fig. 4b). The size compatibility between the circular π-surface of coronene and the partially exposed aromatic regions of **spiro-NG** enables efficient π–π surface complementarity, allowing coronene to act as a supramolecular spacer within the crystal lattice. This interaction leads to the formation of a distinctive hetero-π stacking motif, in which planar coronene molecules are periodically inserted between adjacent **spiro-NG** bilayers. As a result, the crystal structure adopts an alternating stacking arrangement (**spiro-NG**/coronene/**spiro-NG**) along the packing direction. Compared with the crystal packing of pure **spiro-NG**, where bulky *tert*–butyl groups largely suppress intermolecular π-stacking, the presence of coronene effectively mediates intermolecular organization by bridging neighboring bilayer units through π-interactions.

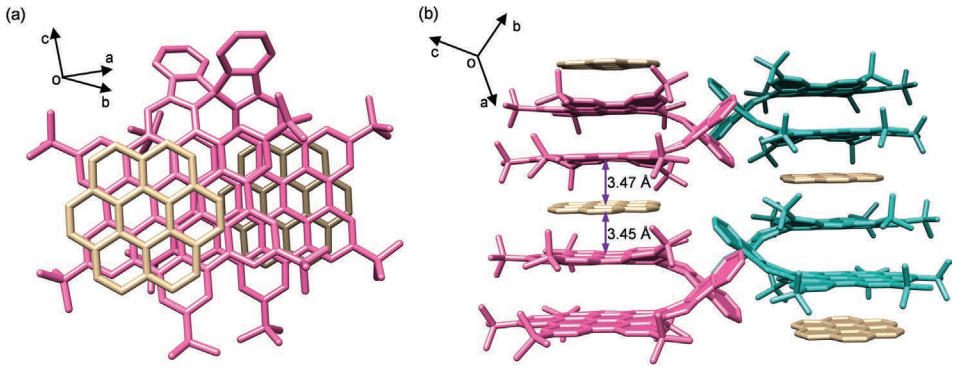


Fig. 4. (a) Top view showing the π-surface recognition between the nanographene (pink) framework and coronene (beige), highlighting the complementary aromatic surface that enables stable host-guest assembly. (b) Side views illustrating the hetero-π–π stacking interactions between the chiral bilayer nanographene and coronene molecules. Coronene intercalates between the two nanographene layers through π–π interactions, forming a sandwich-like stacking motif.

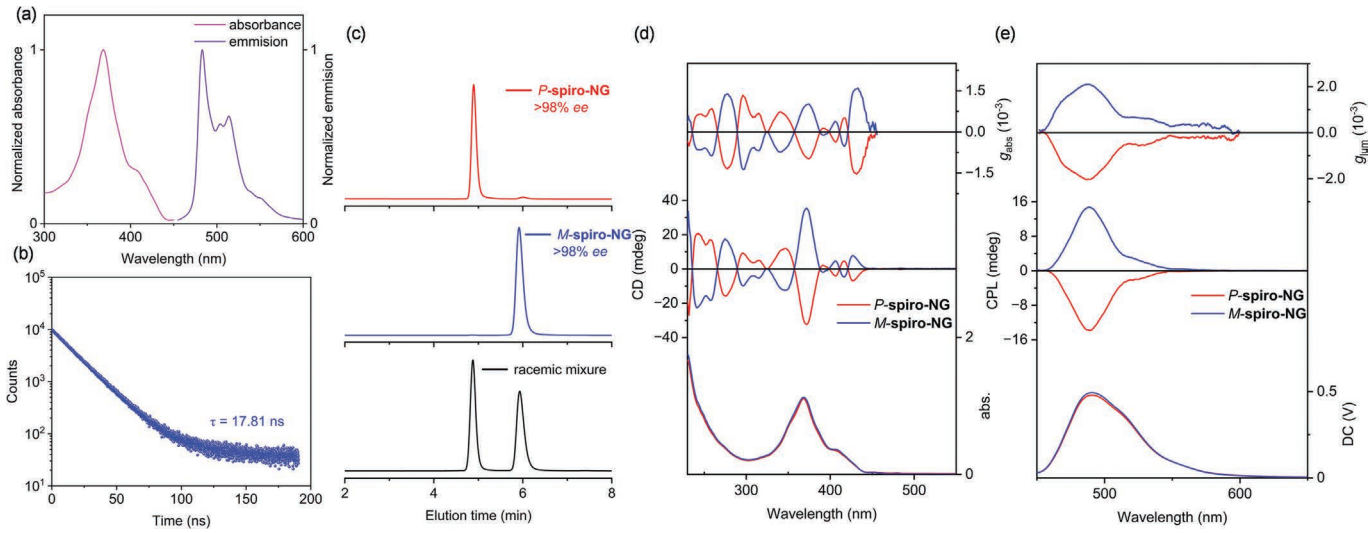


Fig. 5. Photophysical and chiroptical characterization of **spiro-NG**. (a) Normalized absorption and emission spectra of **spiro-NG**. (b) Time-resolved photoluminescence measurement of **spiro-NG** showing a monoexponential decay, which is characteristic of a well-defined molecular fluorescent species. (c) Chiral HPLC chromatograms demonstrate the successful enantioseparation of the racemic mixture (black) into *P*-**spiro-NG** (red) and *M*-**spiro-NG** (blue) using a chiral stationary phase, with both enantiomers achieving over 98 % *ee*. (d) CD and (e) CPL spectra of the resolved *P*-**spiro-NG** (red) and *M*-**spiro-NG** (blue) enantiomers.

Interestingly, the crystal lattice still contains a racemic mixture of *P*- and *M*-**spiro-NG** enantiomers, which assemble into locally homochiral columns along the crystallographic axis. The insertion of coronene molecules appears to promote a more ordered colum-nar organization by reducing steric repulsion between adjacent bilayer nanographenes. From a supramolecular perspective, this observation highlights that planar nanographenes such as coronene can function as effective π-recognition partners, directing the packing of sterically congested bilayer nanographenes through complementary π-surface interactions. These results demonstrate that the extended π-surfaces of **spiro-NG** remain accessible for intermolecular recognition despite the steric protection provided by peripheral *tert*–butyl substituents. The observed nanographene–nanographene π-recognition provides a useful strategy for constructing hetero-π stacked carbon assemblies, which may offer opportunities for tuning electronic coupling and chiroptical properties in supramolecular carbon materials.

The photophysical properties of **spiro-NG** were first investigated in order to elucidate the electronic characteristics of the bilayer nanographene framework. The UV–vis absorption spectrum (Fig. 5a, pink line) exhibits a dominant absorption band centered at 370 nm, which can be assigned to π–π^* transitions within the extended nanographene π-system. The relatively sharp absorption profile and well-resolved spectral features are consistent with the highly rigid and conjugated aromatic framework of the molecule. Upon photoexcitation, **spiro-NG** displays a structured fluorescence band with a maximum at 483 nm (Fig. 5a, purple line). The emission spectrum shows a clear vibronic progression, which is a characteristic feature of rigid polycyclic aromatic hydrocarbons with limited conformational flexibility. Notably, the small Stokes shift between the absorption and emission maxima indicates minimal geometric relaxation in the excited state. This behavior reflects the structural rigidity imposed by the spiro-connected bilayer architecture, which restricts large-scale structural distortion upon excitation. Time-resolved photoluminescence measurements further support this interpretation. As shown in Fig. 5b, the emission decay profile follows a monoexponential behavior with a fluorescence lifetime in the nanosecond regime, suggesting that the excited-state relaxation occurs predominantly through a well-defined radiative pathway from the lowest singlet excited state (S_1). The absence of additional decay components indicates that nonradiative processes such as excimer formation or conformational relaxation are effectively suppressed in this rigid nanographene framework.

Because the two nanographene subunits are connected through a rigid spirobifluorene junction, the overall molecular framework lacks mirror symmetry and therefore possesses intrinsic molecu-

lar chirality. The racemic mixture of **spiro-NG** was successfully resolved by chiral high-performance liquid chromatography (HPLC), affording enantiopure *P*- and *M*-**spiro-NG** with excellent configurational stability (Fig. 5c and Fig. S10 in Supporting information). The CD spectra of the isolated enantiomers display intense mirror-image Cotton effects across the absorption region (Fig. 5d). The rigid spirobifluorene stereocenter locks the two nanographene layers in a stable orthogonal and asymmetric spatial conformation, and the integrated bilayer framework endows the entire conjugated system with excellent chiroptical activity.

Consistent with their strong ground-state chiroptical activity, both enantiomers exhibit clear CPL signals that coincide with the fluorescence maximum at 483 nm (Fig. 5e). The measured dissymmetry factors ($|g_{lum}| \approx 10^{-3}$) fall within the typical range for rigid organic chiral fluorophores. The photoluminescence quantum yield (PLQY) of **spiro-NG** was determined to be 5.58 %, which, combined with the $|g_{lum}|$ value, provides a more complete evaluation of the material's potential for CPL applications in terms of emission brightness and polarization efficiency. These values indicate that the well-defined three-dimensional arrangement of the bilayer nanographene framework creates an effective chiral environment for the emissive excited state. In particular, the spatial coupling between the two π-surfaces may enhance the chiroptical response by amplifying the electric–magnetic transition dipole interactions responsible for CPL activity. Together, these results demonstrate that the spirolinked bilayer architecture not only generates intrinsic molecular chirality but also enables efficient transfer of chiral information to both the ground-state and excited-state optical transitions. Such behavior highlights the potential of bilayer nanographene frameworks as versatile platforms for the development of chiral π-conjugated luminophores with tunable chiroptical properties. To further explore the ability of **spiro-NG** to act as a supramolecular chiral donor, the enantiopure nanographene was co-assembled with achiral fluorescent dyes to form chiral nanoparticles in aqueous media using DSPE-mPEG2000 as an amphiphilic stabilizing matrix. This approach enables the encapsulation of hydrophobic π-conjugated molecules within polymeric nanoassemblies while preserving their photophysical properties (Fig. 6a). The formation of the supramolecular nanoparticles was first examined by dynamic light scattering (DLS) measurements. The DLS results reveal a relatively narrow size distribution with an average hydrodynamic diameter of approximately 243 nm, indicating the formation of well-defined nanoscale assemblies (Fig. 6b). The relatively small polydispersity index further suggests that the nanoparticles possess good colloidal stability in aqueous solution. The morphology of the assemblies was further investigated by scanning electron microscopy (SEM). As shown in Fig. 6c, the nanoparticles exhibit a roughly spherical morphology with diameters of approximately 205–250 nm, which is consistent with the size distribution obtained from DLS analysis. The slightly smaller particle size observed in the SEM images compared with the DLS results can be attributed to the absence of the hydration shell under dry imaging conditions. These results collectively confirm the successful formation of well-defined nanostructures through the supramolecular co-assembly of **spiro-NG** and the guest fluorophores.

Within these nanoconfined assemblies, efficient Förster resonance energy transfer (FRET) from **spiro-NG** to the achiral dye molecules was observed. The photoluminescence spectra show a pronounced decrease in the emission intensity of **spiro-NG** accompanied by the simultaneous emergence of strong fluorescence from the guest dye (Fig. S11 in Supporting information), indicating efficient energy transfer between the two chromophores. Such behavior is consistent with the spectral overlap between the emission of **spiro-NG** and the absorption of the guest fluorophore (Fig. S12 in Supporting information), which satisfies the requirements for FRET. To quantify the FRET process, the FRET efficiency was calculated by comparing the fluorescence lifetimes of the pure donor (**spiro-NG**) and the donor in the donor-acceptor nanoassemblies, affording a FRET efficiency of 46.32 % (17.81 ns for pristine **spiro-NG** *vs.* 9.56 ns for the nanoassemblies, Fig. S13 in Supporting information). Remarkably, the chiral information encoded in the **spiro-NG** donor can be transferred to the achiral

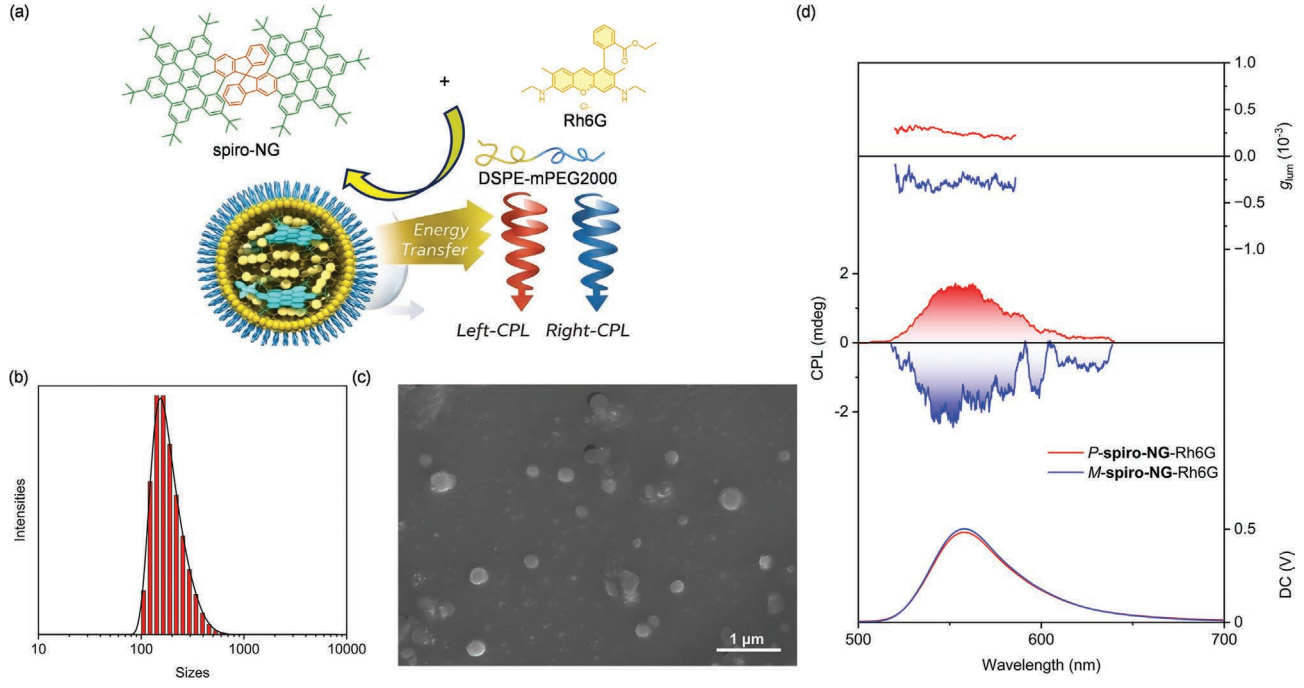


Fig. 6. (a) Molecular structures of **spiro-NG** and Rhodamine 6G (Rh6G) and schematic illustration of the formation of chiral nanoparticles through encapsulation with DSPE-mPEG2000, followed by energy transfer from **spiro-NG** to Rh6G, resulting in left- and right-handed CPL. (b) Dynamic light scattering (DLS) size distribution of the obtained nanoparticles. (c) Scanning electron microscopy (SEM) image of the nanoparticles. Scale bar: 1 μm. (d) Chiroptical and photophysical properties of the nanoparticles, CPL spectra of *P*-**spiro-NG**/Rh6G nanoparticles (red) and *M*-**spiro-NG**/Rh6G nanoparticles (blue).

guest luminophores within the supramolecular assemblies. As shown in Fig. 6d, the nanoparticles display clear CPL signals at the emission wavelength of the guest dye (Rh6G). Importantly, the sign of the induced CPL depends on the handedness of the **spiro-NG** enantiomer used in the assembly, with *P*-**spiro-NG** and *M*-**spiro-NG** producing mirror-image CPL spectra. This observation provides direct evidence for supramolecular chirality transfer from the chiral nanographene donor to the achiral acceptor molecules. Additionally, the PLQY of the donor-acceptor nanoassemblies was determined to be 9.67 %, which complements the chiroptical parameters and further demonstrates the potential of the supramolecular assemblies for CPL-related applications.

The induced CPL signals arise from the chiral environment created by the organized nanographene assemblies, which impose asymmetric electronic coupling between the donor and acceptor chromophores. In such nanoconfined systems, the spatial arrangement of the transition dipole moments enables the transfer of chiral information during the energy-transfer process, leading to circularly polarized emission from otherwise achiral luminophores. Overall, these results demonstrate that bilayer spironanographene can function as an effective supramolecular chiral donor, enabling the construction of nanoparticle systems that combine efficient energy transfer with induced CPL activity. This strategy provides a versatile route toward wavelength-tunable circularly polarized emitters based on chiral nanographene scaffolds.

In summary, we have developed a chiral bilayer spironanographene (**spiro-NG**) that integrates two nanographene subunits through a rigid spirobifluorene junction, providing a well-defined platform for exploring chirality in bilayer carbon nanostructures. Structural analysis by single-crystal X-ray diffraction reveals a folded bilayer architecture in which the two extended π-surfaces are brought into close proximity, enabling effective interlayer electronic communication within a confined framework. The rigid spiro-connected structure endows **spiro-NG** with intrinsic molecular chirality, allowing efficient enantioseparation into *P*- and *M*-enantiomers and the isolated enantiomers exhibit pronounced CD and CPL signals. These results highlight the capability of bilayer nanographene architectures to generate robust chiroptical responses through structural confinement and π-conjugation.

Furthermore, supramolecular co-assembly of **spiro-NG** with achiral fluorophores in nanoconfined environments enables chirality transfer *via* Förster resonance energy transfer, giving rise to induced circularly polarized emission from guest luminophores. This strategy provides a versatile route toward wavelength-tunable CPL systems based on chiral nanographene donors. Overall, this work demonstrates that bilayer spironanographene constitutes an effective chiral nanographene scaffold that combines well-defined molecular chirality with supramolecular chiroptical functionality. These findings provide new insights into the design of chiral π-conjugated nanostructures and offer promising opportunities for developing carbon-based chiral photonic materials and optoelectronic devices.

CRediT authorship contribution statement

Zhaoyu Yan: Software, Investigation, Formal analysis, Data curation. **Yuanhao Feng:** Visualization, Software. **Zhewen Ma:** Visualization, Software. **Wei Zheng:** Writing – review & editing, Writing – original draft, Visualization, Resources, Project administration, Funding acquisition, Conceptualization.

Declaration of competing interest

The authors declare that they have no known competing financial interests or personal relationships that could have appeared to influence the work reported in this paper.

Acknowledgments

This work was partially supported by the National Natural Science Foundation of China (NSFC, Nos. 22301220, 22471199 (W. Zheng)), as well as the Fundamental Research Funds for the Central Universities. Y. Feng acknowledged the financial support from the China Scholarship Council (No. 202506260039).

Supplementary materials

Supplementary material associated with this article can be found, in the online version, at doi:10.1016/j.cclet.2026.112890.

References

[1] P. Izquierdo-García, J. Lión-Villar, J.M. Fernández-García, et al., Chem. Soc. Rev. 54 (2025) 11089–11104.
[2] P.J. Evans, J. Ouyang, L. Favereau, et al., Angew. Chem. Int. Ed. 57 (2018) 6774–6779.
[3] T. Ohta, J.T. Robinson, P.J. Feibelman, et al., Phys. Rev. Lett. 109 (2012) 186807.
[4] K. Liu, L. Zhang, T. Cao, et al., Nat. Commun. 5 (2014) 4966.
[5] M. Kolmer, W. Ko, J. Hall, et al., J. Phys. Chem. Lett. 13 (2022) 11571–11580.
[6] P. Izquierdo-García, J.M. Fernández-García, S.M. Rivero, et al., J. Am. Chem. Soc. 145 (2023) 11599–11610.
[7] P. Izquierdo-García, J.M. Fernández-García, J. Perles, et al., J. Am. Chem. Soc. 146 (2024) 34943–34949.
[8] Y. Zhu, M.A. Petrukhina, Chem. Soc. Rev. 55 (2026) 3061–3077.
[9] W. Wang, P. Sun, X. Liu, et al., Org. Lett. 26 (2024) 1017–1021.
[10] M.A. Niyas, K. Shoyama, M. Grüne, et al., Nature 637 (2025) 854–859.
[11] Z. Zhou, J.M. Fernández-García, Y. Zhu, et al., Angew. Chem. Int. Ed. 61 (2022) e202115747.
[12] X.J. Zhao, H. Hou, X.T. Fan, et al., Nat. Commun. 10 (2019) 3057.
[13] P. Izquierdo-García, J.M. Fernández-García, N. Martín, J. Am. Chem. Soc. 146 (2024) 32222–32234.
[14] J.M. Fernández-García, P.J. Evans, S. Filippone, et al., Acc. Chem. Res. 52 (2019) 1565–1574.
[15] W. Niu, Y. Fu, Z.L. Qiu, et al., J. Am. Chem. Soc. 145 (2023) 26824–26832.
[16] W. Niu, Y. Fu, Q. Deng, et al., Angew. Chem. Int. Ed. 63 (2024) e202319874.
[17] M. Liu, L. Zhang, T. Wang, Chem. Rev. 115 (2015) 7304–7397.
[18] T. Fujikawa, Y. Segawa, K. Itami, J. Am. Chem. Soc. 137 (2015) 7763–7768.
[19] H.V. Anderson, N.D. Gois, W.A. Chalifoux, Org. Chem. Front. 10 (2023) 4167–4197.
[20] V. Kumar, J.L. Páez, S. Míguez-Lago, et al., Chem. Soc. Rev. 54 (2025) 4922–4947.
[21] N.T. Yao, Y.J. Shen, Y. Wu, et al., Org. Lett. 27 (2025) 9253–9258.
[22] J. Labella, W.R. Osterloh, K. Kuo, et al., J. Am. Chem. Soc. 148 (2026) 9670–9679.
[23] J.K. Li, X.Y. Chen, W.L. Zhao, et al., Angew. Chem. Int. Ed. 62 (2023) e202215367.
[24] M. Reale, E. Marino, E. Maçôas, et al., Adv. Funct. Mater. 34 (2024) 2402079.
[25] Y. Zhang, S. Yu, B. Han, et al., Matter 5 (2022) 837–875.
[26] L. Zhou, G. Liu, Y. Han, et al., J. Am. Chem. Soc. 148 (2026) 8585–8595.
[27] Z. Sun, Q. Ye, C. Chi, et al., Chem. Soc. Rev. 41 (2012) 7857–7889.
[28] J. Meng, D. Shi, G. Zhang, Mod. Phys. Lett. B 28 (2014) 1430009.
[29] E. Jin, Q. Yang, C.W. Ju, et al., J. Am. Chem. Soc. 143 (2021) 10403–10412.
[30] X. Zhang, X. Ge, J. You, et al., J. Mater. Chem. C 13 (2025) 20444–20462.
[31] Y. Han, Z. Xue, G. Li, et al., Angew. Chem. Int. Ed. 59 (2020) 9026–9031.
[32] G.F. Huo, W.T. Xu, J. Hu, et al., Angew. Chem. Int. Ed. 64 (2025) e202416707.
[33] W. Cui, Z. Jin, W. Fu, et al., Chin. Chem. Lett. 35 (2024) 109667.
[34] H. Shi, B. Xiong, Y. Chen, et al., Chin. Chem. Lett. 34 (2023) 107520.
[35] W. Fan, T. Matsuno, Y. Han, et al., J. Am. Chem. Soc. 143 (2021) 15924–15929.
[36] J. Hu, Q. Xiang, X. Tian, et al., J. Am. Chem. Soc. 146 (2024) 10321–10330.
[37] C. Li, Y. Ma, J. Yu, et al., Chin. Chem. Lett. 37 (2026) 111719.
[38] W. Yu, C. Yang, X. Feng, et al., Chin. Chem. Lett. 36 (2025) 110939.
[39] J.F. Xing, K. Li, W. Xiang, et al., Chin. Chem. Lett. 36 (2025) 110982.
[40] X. Liu, Z. Jin, F. Qiu, et al., Angew. Chem. Int. Ed. 63 (2024) e202407547.
[41] B. Li, W. Peng, S. Luo, et al., Org. Lett. 21 (2019) 1417–1421.
[42] P. Izquierdo-García, J.M. Fernández-García, J. Perles, et al., Angew. Chem. Int. Ed. 62 (2023) e202215655.
[43] V. Kumar, S.D. Dongre, A. Vandhanam, et al., J. Phys. Chem. Lett. 16 (2025) 11657–11664.
[44] S. Liu, D. Xia, M. Baumgarten, ChemPlusChem 86 (2021) 36–48.
[45] T.P.I. Saragi, T. Spehr, A. Siebert, et al., Chem. Rev. 107 (2007) 1011–1065.
[46] S.Q. Song, X. Han, Z.Z. Huo, et al., Sci. China Chem. 67 (2024) 2257–2264.
[47] T. Sakamaki, Y. Zhang, S. Fukuma, et al., J. Am. Chem. Soc. 146 (2024) 12712–12722.
[48] J. Shang, Z. Wang, C. Sun, et al., Angew. Chem. Int. Ed. 63 (2024) e202414231.
[49] Z. Zhang, D. Csókás, I. Fernández, et al., Chem 10 (2024) 3199–3211.
[50] B. Yang, Y. Sun, J. Hu, et al., Chem 11 (2025) 102628.
[51] M. Buendía, A.J. Stasyuk, S. Filippone, et al., Org. Chem. Front. 12 (2025) 1438–1443.
[52] Y. Saegusa, T. Ishizuka, T. Kojima, et al., Chem. Eur. J. 21 (2015) 5302–5306.

[53] B. Pigulski, K. Shoyama, M.-J. Sun, et al., J. Am. Chem. Soc. 144 (2022) 5718–5722.
[54] P. Ximenis, D. Martínez, L. Rubert, et al., Chem. Soc. Rev. 54 (2025) 11659–11698.
[55] M. Mahl, M.A. Niyas, K. Shoyama, et al., Nat. Chem. 14 (2022) 457–462.
[56] M.A. Niyas, K. Shoyama, F. Würthner, Angew. Chem. Int. Ed. 62 (2023) e202302032.
[57] M.A. Niyas, S. Garain, K. Shoyama, et al., Angew. Chem. Int. Ed. 63 (2024) e202406353.
[58] M.A. Niyas, K. Shoyama, F. Würthner, J. Am. Chem. Soc. 146 (2024) 29728–29734.
[59] S. Huang, H. Yu, Q. Li, Adv. Sci. 8 (2021) 2002132.
[60] Z.X. Lian, X.Z. Wang, C.W. Zhou, et al., Chin. Chem. Lett. 35 (2024) 109063.
[61] R. Ren, Y. Pan, H.X. Wang, et al., Chin. Chem. Lett. 37 (2026) 111060.
[62] S. Jiang, S. Zhou, Y. Chen, et al., Chin. Chem. Lett. 33 (2022) 2442–2446.
[63] T. Zhao, J. Han, P. Duan, et al., Acc. Chem. Res. 53 (2020) 1279–1292.
[64] R. Zhang, H. Zhong, K. Yang, et al., Adv. Funct. Mater. 35 (2025) 2417308.
[65] Y. Zhang, Y. Han, S. Yuan, et al., Nat. Commun. 16 (2025) 5862.
[66] H.Q. Peng, L.Y. Niu, Y.Z. Chen, et al., Chem. Rev. 115 (2015) 7502–7542.
[67] J. Lión-Villar, H.S. Torchon, Y. Zhu, et al., Angew. Chem. Int. Ed. 64 (2025) e202510209.